Structure and Properties of Ti⁴⁺-Ureasil Organic-Inorganic Hybrids

Celso Molina,[a] Karim Dahmouche,[a] Peter Hammer,[a] Verónica de Zea Bermudez,[b] Luís D. Carlos,[c] Maurizio Ferrari,[d] Maurizio Montagna,[e] Rogéria R. Gonçalves,[f] Luiz. F. C. de Oliveira,[g] Howell. G. M. Edwards,[h] Younes Messaddeq[a] and Sidney J. L. Ribeiro[,a]*

[a]*Instituto de Química, Universidade Estadual Paulista, CP 355, 14801- 970 Araraquara – SP, Brazil*

[b]*Departamento de Química, Universidade de Trás-os-Montes e Alto Douro, Quinta dos Prados, 5001 Vila Real Codex, Portugal*

[c]*Departamento de Física, Universidade de Aveiro, 3810 Aveiro, Portugal*

[d]*CNR-INF, Instituto di Fotonica i Nanotecnologie, CSMFO Group, via Sommarive 14, 38050, Povo (TN), Italy*

[e]*IDipartimento di Fisica, Università di Trento, CSMFO Group, via Sommarive 14, 38050 Povo, (TN), Italy*

[f]*Departamento de Química, Universidade de São Paulo, 14040-901 Ribeirão Preto – SP, Brazil*

[g]*Departamento de Quimica, Universidade Federal de Juiz de Fora, 36036-900 Juiz de Fora – MG, Brazil*

[h]*Department of Chemical and Forensic Sciences, University of Bradford, Bradford, BD7 1 DP, UK*

Guias de luz planares foram obtidos a partir de um sol de um novo híbrido Ti⁴⁺-acetilacetona (acac)-Ureasil depositado na forma de filmes finos sobre substratos de vidro. A estrutura foi investigada por medidas espectroscópicas (absorção no infravermelho, fotoelétrons de raios-X e espalhamento Raman) e espalhamento de raios-X a baixos ângulos (SAXS). Para a adição do complexo Ti-acac ao ureasil na razão molar Ti:Si de 1:1 interações entre o complexo Ti-acac e grupos siloxanos foram identificadas. Quantidades maiores de Ti⁴⁺ (razão molar Ti:Si de 5:1) levam também à formação de nanoagregados ricos em titânio. Os parâmetros ópticos dos guias, como índice de refração, espessura, modos propagados e coeficiente de atenuação foram medidos para 632,8, 543,5 e 1550 nm pela técnica de acoplamento de prisma. O índice de refração pode ser controlado pela quantidade relativa de titânio. Guias de poucos micra de espessura suportam modos de propagação com baixas perdas para todas as composições.

Hybrid planar waveguides were prepared from Ti⁴⁺-acetylacetone (acac)-Ureasil sols deposited on glass substrates. Structural features have been investigated by spectroscopic measurements (Fourier Transform Infrared Spectroscopy (FTIR), X-ray Photoelectron Spectroscopy (XPS) and Raman scattering) and Small Angle X-ray Scattering (SAXS). Addition of Ti⁴⁺-acac to the ureasil (Ti:Si molar ratio 1:1) leads to the formation of bonds between the Ti complex and the siloxane groups, whereas further addition of Ti⁴⁺ (Ti:Si molar ratio 5:1) leads to the additional formation of titanium-rich nanoclusters. The optical parameters of the waveguides such as refractive index, thickness, propagating modes and attenuation coefficient were measured at 632.8, 543.5 and 1550 nm by the prism coupling technique. The refractive index can be tuned by the Ti⁴⁺ relative content. The few microns thick planar waveguides support well confined propagating modes with low attenuation loss for all compositions.

Keywords: planar waveguides, sol-gel, hybrid materials, ureasil

Introduction

The sol-gel route has led to innovative hybrid organic/inorganic frameworks where the conjunction of the appropriate processing conditions with the adequate choice of the organic and inorganic components primarily determines the morphology, molecular structure and properties of the xerogels.[1,2] The major driving force behind the intense activity in this expanding area of materials science research is

* e-mail: sidney@iq.unesp.br

undoubtedly the possibility of developing nanoscale systems with a variety of features that cannot be normally found in conventional macroscale composites or in traditional materials. The scope of application of nanohybrids is extraordinary, as they may find use in domains as diverse as electrochemistry, biology, mechanics, ceramics, electronics and optics.[3]

In previous works we synthesized the sol-gel derived host network, termed di-ureasil, which comprises polyether-based chains of variable length covalently bonded on both ends to a siliceous backbone through urea functionalities (-NHC(=O)NH-).[4] These systems can be represented by U(Y) (with Y = 2000, 900 and 600), where U represents the urea group and Y denotes the average molecular weight of the organic precursor used.

These di-ureasils display several remarkable properties. From the point of view of preparation the xerogels are easily obtained as thin, elastomeric and highly transparent monoliths, thermally stable up to 220 ºC. From the electrochemical standpoint, as they are essentially amorphous (a necessary condition for ion transport), the observed conductivity values in alkaline-doped di-ureasils are very similar to those found in the classical polyether-based electrolytes (up to 10^{-4} S/cm^{-1}).[5] Unlike the latter materials, the di-ureasils offer the advantage of being able to accommodate considerably larger amounts of guest salt, thus preventing the undesired "salting out" phenomenon to occur and exhibit better mechanical and thermal properties than the siloxane-free polymeric ionic conductors.

The urea cross-linked silicates will presumably find application also in the field of optics due to their quite outstanding optical features. We have demonstrated that, apart from being white-light emitters, the color emitted by the Eu^{3+}-doped di-ureasils may be readily tuned across the CIE (Commission Internationale d'Éclairage) chromaticity diagram by varying either the salt concentration or the excitation wavelength.[6] Concerning the coordination properties towards trivalent optically active rare earth ions we have shown various interesting characteristics as a function of the organic counterpart chain length. In the U(2000)-based materials, which contain polymer segments with approximately 40.5 oxyethylene repeat units, lanthanide trivalent ions are preferentially coordinated by the oxygen atoms of the urea carbonyl groups instead of to the oxygen atoms of the polyether chains. This picture remains valid as long as the saturation of the urea coordinating sites is not attained, a situation that only occurs for n = 20 (where n is the ratio of OCH$_2$CH$_2$ units per Eu^{3+} ion). At that specific salt concentration

the number of available urea cross-links groups per lanthanide cation will be 1 (this composition could be also denoted as n'= 1, where n' is the ratio of Si atoms per Eu^{3+} ion). At higher salt concentration, as no carbonyl groups are left free, the ether-type oxygen atoms of the polymer segments ensure the complexation of the additional lanthanide ions. A stoichiometric crystalline complex is formed at n < 5.

Analogous materials containing shorter polyether segments display completely different coordination characteristics. The inclusion of shorter polymer chains in the di-ureasil-type structure results in the formation of a hybrid framework with a larger number of cross-links. In practice, this effect results primarily in a shift of the urea saturation composition to higher salt content. Previous FT-IR and luminescence spectroscopy studies corroborate that urea linkages are not involved in the coordination of the Eu^{3+} ions at low concentration.[7] In these short-chain di-ureasils the cations are preferentially bonded to the ether oxygen atoms of the organic segments. Both coordination environments (i.e., Eu^{3+} ⋯O=C(urea) and Eu^{3+} ⋯OCC(polymer) are, however, present in the low to medium salt concentration range when a host matrix containing low molecular weight polymer segments, such as U(600) (containing 8.5 oxyethylene repeat units) is used.

The tunability of the coordination process in the di-ureasils through the control of the guest salt concentration and the polymer chain length is extremely attractive, both from the fundamental and technological standpoint.

Due to the fact that thick and resistant deposits can be easily obtained, Ureasils are also foreseen as waveguides in the field of optics. For this application the control of refractive index of the hybrid coatings deposited on glass substrates or silicon wafers, through the incorporation of different amounts of a dopant, would be desirable. The aim of this work is two fold: First, to synthesize novel Ti^{4+}-containing Ureasil waveguides whose refractive index can be controlled by the titanium content and second, to understand how the incorporated Ti^{4+} ions affect the local and nanoscopic structure of the material.

Experimental

Synthesis

All the chemicals used in the synthesis procedure described below were purchased from Fluka and Aldrich. The di-ureasil host matrix contains short (CH$_2$CH$_2$O)-based polymer chains whose ends are grafted to a siliceous

network by means of urea linkages. The cross-links between the organic and the inorganic components were formed by reacting the NH_2 groups of a diamine (chemically α,ω-diaminepoly(oxyethylene-co-oxypropylene) and commercially Jeffamine-ED600®) with the -N=C=O group of 3-isocyanatepropyltriethoxysilane, ICPTES, in tetra-hydrofuran, THF, under reflux at 80 °C for 6 hours.[4,6,7] The precursor of U(600) (termed ureapropyltriethoxysilane, UPTES) was isolated after evaporating the solvent. The stable Ti^{4+} based sol was prepared by mixing equimolar quantities of tetraisopropoxytitanate $[Ti(OPr^i)_4]$ and acetylacetone (acac). The titanium sol was added to the ureasil precursor in different Ti:Si molar ratios. Samples are identified by the designation $U(600)Ti_x$, where U originates from the word "urea", 600 indicates the average molecular weight of the diamine used and x = 1, 3 and 5 represents the Ti:Si molar ratio. Ammonium fluoride, NH_4F, dissolved in ethanol and water were then added to UPTES and Ti sol mixture to catalyze the hydrolysis reaction of the alkoxy groups. Hybrid films were deposited by dip-coating on sodalime glass substrates and silicon wafers at a withdrawn speed of 95 mm min⁻¹. Then the films were dried at 80 °C for 24 h.

XPS measurements

Samples deposited on silicon wafers were transferred into the XPS chamber and measured immediately without further treatment. The Al $K_α$ line (1486.6 eV, width 0.85 eV) and the analyzer pass energy of 10 eV were used (VG-Escalab not monochromated). After the subtraction of the elastic background of the C 1s and O 1s, N 1s, Si 2p and Ti 2p electron core-level spectra the composition was determined from the ratio of the relative peak areas corrected by sensitivity factors of the corresponding elements. Further examination of the spectra was performed by a multiple Voigt profile peak fitting procedure.

Infrared spectroscopy

Mid-infrared spectra were acquired at room temperature using a FTIR Perkin Elmer Spectrometer Spectrum 2000 system. The spectra were collected over the range 4000-400 cm⁻¹, by averaging 32 scans at a maximum resolution of 4 cm⁻¹. Before analysis the solid samples (2 mg) were finely milled, dispersed in approximately 175 mg of spectroscopic grade potassium bromide (KBr, Merck), pressed to pellets and then introduced into a dessicator over P_2O_5 for at least 12 h at room temperature in order to reduce the levels of adsorbed water. In order to evaluate the measured complex band envelopes and to identify underlying spectral components a deconvolution procedure was performed using Gaussian peak shapes.

Raman scattering

FT-Raman spectra were excited at 1064 nm using a Nd:YAG laser and a Bruker IFS66 optical bench with a FRA 106 Raman accessory containing a liquid-nitrogen cooled germanium detector. Laser power was kept at 300 mW (about 100 mW at the sample) and 2000 scans were accumulated with a spectral resolution of 4.0 cm⁻¹, using the 180° scattering geometry, from 100 to 4000 cm⁻¹.

Optical parameters of the waveguides

The refractive index and the thickness of the waveguides were measured for both transverse electric (TE) and transverse magnetic (TM) polarization with an m-line apparatus (Metricon mod. 2010) based on the prism coupling technique. The refractive index of the gadolinium gallium garnet (GGG) prism was 1.9644 at 632.8 nm. The apparatus was equipped with Si and Ge detectors to collect the visible and NIR light, respectively. Two He-Ne lasers, operating at 632.8 and 543.5 nm and one diode laser operating at 1550 nm were employed. The resolution in the determination of the angles synchronous to the propagation modes was 0.0075°. In order to measure propagation losses the light intensity scattered out of the waveguide plane was recorded by scanning down the length of the propagating streak using a fiber probe. The losses were evaluated by fitting the intensity by an exponential decay function, assuming a homogeneous distribution of the scattering centers in the waveguide. The measurements were performed, by exciting the transverse electric mode (TE_0) of the waveguide at 632.8 and 1550 nm.

SAXS

The SAXS experiments were performed at the SAXS synchrotron beamline of LNLS (National Synchrotron Light Laboratory, Campinas, Brazil). The beamline was equipped with an asymmetrically cut and bent silicon (111) monochromator that yielded a monochromatic (λ = 1.608Å) and horizontally focused beam. A vertical position-sensitive X-ray detector and a multichannel analyser were used to record the SAXS intensity, I(q), as a function of the modulus of scattering vector q = 4πsin(θ/λ), θ being the half of the scattering angle. Each SAXS spectrum was collected over a time interval of 300 s. Because of the small size of the

incident beam cross section at the detection plane, no mathematical desmearing of the experimental SAXS function was needed. A constant intensity background due to short-range electron density fluctuations was removed from the experimental scattering profile.

Results and Discussion

The hydrolysis and condensation of the di-ureasil precursor is well known and studied in previous papers.[4,6,7] The structural features of the homogenous and transparent samples are well described by polyether-based chains grafted at the two sides to siliceous nanodomains, which sizes and distances were observed to be controlled by the size of the polymeric counterpart. With the addition of the Ti-acac complex to the di-ureasils yellowish sols were obtained for all compositions. The hydrolysis/ condensation of the mixture could lead to different products including co-condensation of the metal alkoxides or phase separated samples at the molecular level. As it will be discussed in the following the contribution of both process could be considered depending on relative concentrations. Homogeneous, few microns thick films were obtained from the dip-coating process either on the soda-lime glass or silicon substrates. Favorable waveguiding properties have been observed as it will be discussed in the following.

Vibrational spectra

Raman spectra obtained for the di-ureasil U(600) (Figure1(a)) and the new hybrids U(600)Ti$_1$, U(600)Ti$_3$ and U(600)Ti$_5$ (Figure 1(d-f)) are displayed in Figure 1. Included are also spectra of two other samples prepared for comparison purposes. The first one (Figure 1(b)) was obtained from the hydrolysis of Ti(OPr^i)$_4$ followed by heat treatment of the powdered sample at 300 ^{o}C for 24 h. The characteristic anatase bands of this TiO$_2$ phase can be observed at 638 cm^{-1} (v_1- E$_g$ mode), 518 cm^{-1} (v_2+v_3- B$_{1g}$+A$_{1g}$ modes), 401 cm^{-1} with a shoulder at 369 cm^{-1}-(v_4-B$_{1g}$ mode) and 149 cm^{-1} (v_6- E$_g$ mode). The second sample (Figure 1(c)) is a xerogel prepared from the hydrolisys/condensation of the acac stabilized Ti^{4+} sol and then dried at 80 ^{o}C for 2h. Figure 1 shows that the contribution of the bands observed for the pure Ti^{4+}- acac sample is still present and increases in intensity with the increase of the Ti^{4+} concentration in the hybrids. Of special interest is the group of three main bands appearing for Ti^{4+}-acac xerogel at 668, 563-545 (doublet) and 448 (with a shoulder at 415) cm^{-1}. In comparison with the spectrum obtained for the pure anatase the group

of 3 bands observed for the Ti-acac xerogel are shifted to higher wavenumbers. These bands could be related to similar Ti^{4+} local structures in the xerogel and the anatase phase.
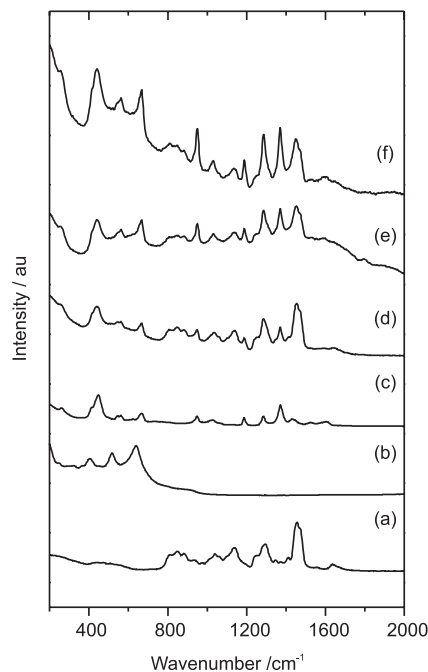

Figure 1. Raman spectra. (a) U(600); (b) Hydrolyzed Ti(OPr^i)$_4$ heat-treated at 300 ^{o}C for 24 h; (c) acac stabilized Ti^{4+} sol dried at 80 ^{o}C for 2h; (d) U(600)Ti$_1$; (e) U(600)Ti$_3$ and (f) U(600)Ti$_5$.

Infrared absorption spectra are displayed in Figure 2 for the pure U(600) sample (Figure 2(a)), the Ti-acac xerogel (Figure 2(b)), the U(600)Ti$_1$ and the U(600)Ti$_5$ samples (Figure 2(c) and (d) respectively). As already observed in Raman spectra there is an increasing contribution from the characteristic bands observed for the Ti-acac xerogel (Figure 2(b)) as the relative concentration of Ti-acac in the hybrids increases.

The full analysis of the infrared spectra obtained for the di-ureasils can be found elsewhere.[4,7] A tentative Gaussian deconvolution was performed for the 1450-1850 cm^{-1} range in order to extract more structural information and Figure 3 shows the results so obtained.

In this region the so-called Amide I and Amide II bands - a pair of spectral features produced by the urea cross-links - yield extremely rich information, not only about the process of cation complexation in the di-ureasils but also about the extent and strength of hydrogen bonding throughout the materials.[4] The Amide I band (1600-1750 cm^{-1}) appears usually as a broad and complex envelope composed of several components including C-N-C stretching and the C-C-N deformation vibration modes and C=O stretching groups free from any interaction or involved in hydrogen bonded associations
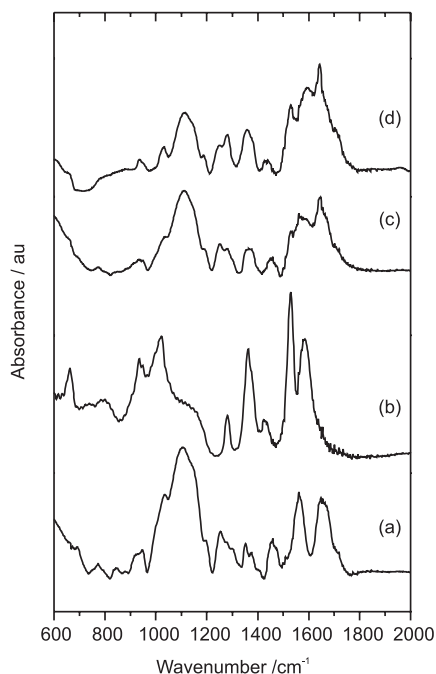
Figure 2. FT-IR absorption spectra. (a) U(600); (b) acac stabilized Ti⁴⁺ sol dried at 80 ºC for 2h; (c) U(600)Ti₁ and (d) U(600)Ti₅.
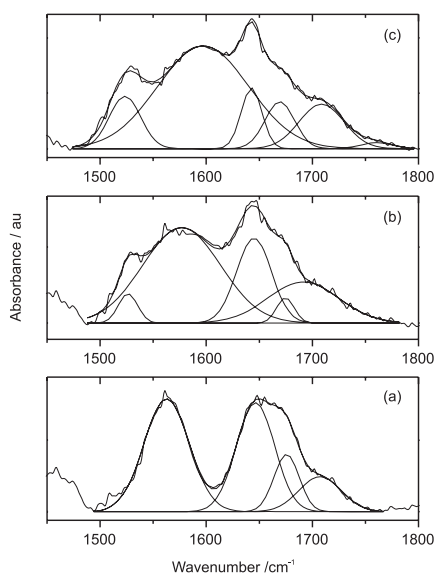

Figure 3. FT-IR absorption spectra (deconvolution results). (a) U(600); (b) U(600)Ti₁ and (c) U(600)Ti₅.

of variable strength. We have shown that the individual components found in the Amide I envelope of the di-ureasil hybrids reflect the presence of more or less ordered hydrogen-bonded structures involving the interaction between the N-H moieties of the urea linkages and the carbonyl oxygen of a neighboring urea group or the ether oxygen of the polymer segments.[4,7] Considering the U(600) hybrid three components at 1707, 1677 and 1645 cm⁻¹ are observed in Figure 3(a). Due to the relative high number of urea moieties present, the formation of strong

and ordered self-associated urea-urea interactions dominates in U(600), producing the intense component at 1645 cm⁻¹. The absence of an individual band at 1750 cm⁻¹ in the spectrum of U(600) suggests that the extension of hydrogen bonding throughout the material is such that neither C=O nor N-H groups are left free.[7] The other two components of the Amide I absorption band of U(600) are attributed to the formation of a minor number of less ordered urea-polyether associations.

In the spectra of U(600)Ti hybrids shown in Figure 3(b) and 3(c) the Amide II band appearing as a broad band at 1564 cm⁻¹ is completely masked by bands related to the Ti⁴⁺-acac complex at 1529 and 1582 cm⁻¹. However in the Amide I band region, with the increase in Ti⁴⁺ concentration an increase is observed for the component at 1643 cm⁻¹. As that component could be assigned to Urea-Urea interactions, the presence of Ti⁴⁺ seems to increase this kind of association at the expenses of Urea-Polyether interaction. In fact in the spectral region corresponding to C-O polyether bonds only a small blue shift (1102 cm⁻¹ observed for the pure U(600) to 1110 cm⁻¹ found for the U(600)Ti₅ sample) together with the narrowing of the band are observed, which could be a sign of the disruption of the Urea-polyether associations. This information is useful in order to understand some of the XPS and SAXS features shown below.

X-ray Photoelectron Spectroscopy (XPS)

The nominal elemental composition and the results obtained by the XPS analysis for the U(600) sample are compared in Table 1. A good agreement is observed between the nominal atomic fractions of elements in the hybrid, derived from the molecular stoichiometry (Mol.U600 in the table), and the experimental XPS values (XPSU600 in the table). The corrected N 1s intensity was chosen to normalize the concentration values of the other elements since there is a constant fraction of bonded nitrogen in the U600 molecule and the signal to noise ratio is higher than that detected for the Si 2p peak. Table 1 displays also the element to nitrogen ratios [X/N] (X = C, O, Si, Ti) of the studied samples. The data show that the addition of the Ti-acac complex increases the titanium concentration from 2.6 at.% (sample U(600)Ti₁) to 6.8 at.% (sample U(600)Ti₅) and also rises the fraction of total carbon (up to 50%) and oxygen (up to 64%).

The deconvoluted C 1s, O 1s and Si 2p core-level spectra are displayed in Figure 4 (a-c) for the U(600) hybrid and the U(600)Ti₁ and U(600)Ti₅ samples, respectively.

For the pure hybrid film the three identified C 1s components could be assigned to: C-N, C-C and C-Si-O

Table 1. Number of atoms and atomic fractions of elements in the U(600) hybrid compared with XPS results and element to nitrogen ratio [X/N] of the U(600) hybrid compared with the ratios obtained by XPS for different Ti^{4+} concentrations

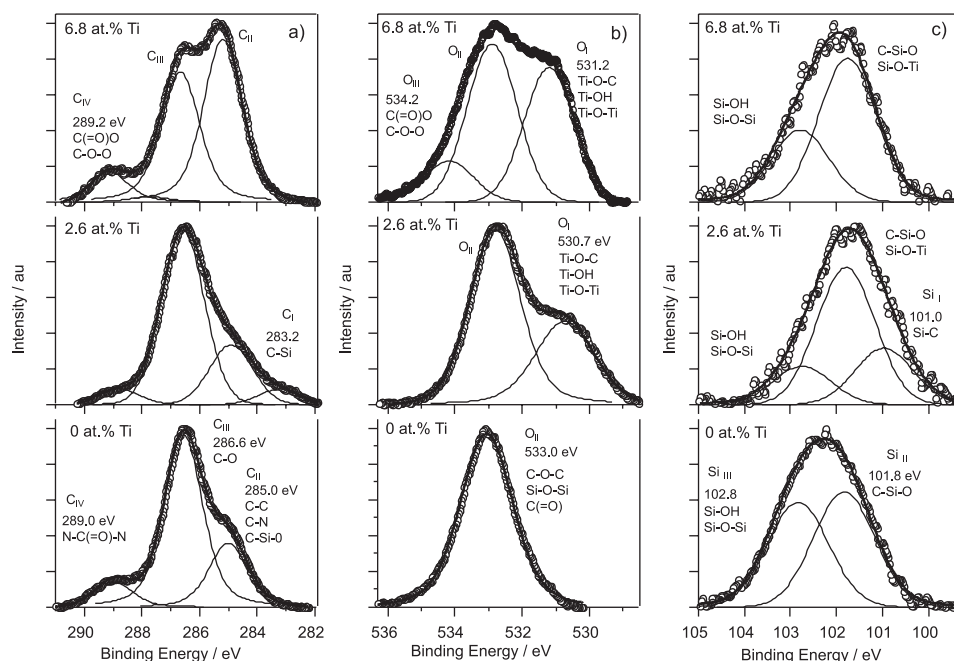| Element X	Mol.U600		XPS U600		[X/N] Mol. U600	[X/N] XPS at.%Ti			
	atoms	at.%	atoms	at.%		0.0	2.6	5.6	6.8
C	35.5	61.7	35.0	60.8	8.9	8.9	11.9	16.1	17.5
O	16.0	27.8	15.9	27.6	4.0	4.1	6.0	10.2	11.0
N	4.0	6.9	3.9	6.8	-	-	-	-	-
Si	2.0	3.5	2.7	4.7	0.5	0.6	0.6	0.5	0.7
Ti	-	-	-	-	-	-	0.5	1.7	2.2

Figure 4. XPS deconvoluted C 1s (a), O 1s (b) and Si 2p (c) core-level spectra for the undoped hybrid and titanium-doped samples U(600)Ti$_1$, U(600)Ti$_3$ and U(600)Ti$_5$.

at about 285.0 eV (denoted as C_{II}); C-O bonds at 286.6 eV (denoted as C_{III}) and to the urea C=O structure (NC(=O)N) at 289.0 eV (denoted as C_{IV}).[8]

The O 1s spectrum shows a rather symmetric peak at 533.0 eV (O_{II}) attributed to the C-O, -Si-O-Si and C(=O) structures, present in the U(600) hybrid.[8]

The analysis of the Si 2p peak reveals that the silicon is bonded to terminating OH groups or in Si-O-Si structures at about 102.8 eV (denoted as SiIV) and in siloxane groups of U(600) located at 101.8 eV (denoted as SiII). From this result a network connectivity (C-Si-O-Si-C structures) of the hybrid is estimated to be higher than 60%.

The C 1s spectrum of the U(600)Ti$_1$ sample displays a small increase of the C_{III} (C-O) component and a small component emerges at 283.2 eV (denoted as C_I). The increase of the C_{III} component accounts for the additional C-O bonds introduced by the Ti^{4+}-acac complex. A new component observed in the O 1s spectrum at 530.7 eV

(O_I) is attributed to Ti-O-C and Ti-OH.[9,10] In addition, $_{3/2}$OTiOTiO$_{3/2}$ groups formed as by-product of Ti^{4+}-acac complex are expected to contribute at about 530.5 eV. This binding energy is somewhat higher than that for pure TiO_2 bonds, expected at about 530 eV.[8] The added Ti^{4+} complex undergoing hydrolysis should lead to Ti-OH based species and free acetylacetone molecules. The emergence of C_I suggests the interaction of the Ti^{4+} complex with Si^{4+} of the siloxane group. In fact chemical equilibrium involving the formation of species formed by acac molecules coordinating to Si^{4+} can not be discarded. This interpretation is compatible with the results of the Si 2p peak analysis indicating the possible presence of such bonds at 101.0 eV (denoted as Si_I). Furthermore, also the formation of direct Ti-O-Si bonds, expected at 101.7 eV (Si 2p peak), must be considered (Figure 4(c)).

At higher titanium concentration (sample U(600)Ti$_5$) pronounced structural changes take place: *i*) From the C 1s

spectra a strong increase of hydrocarbon groups contributing to C_{II} is observed. The contribution of the peak attributed to C(=O)O groups with a characteristic peak at 289.2 eV (C_{IV}) can also be identified. *ii*) In the O 1s spectrum the presence of the later structures is responsible for the increased contribution of the component at 534.2 eV (O_{III}). The shift of the O_I peak to higher binding energy (531.2 eV) occurs most probably due to additional contribution of Ti-OH groups. *iii*) In the Si 2p spectrum the low energy shoulder (SiC_x) disappears and the changed ratio of the components suggests a doping induced decrease of the hybrid connectivity down to 33%. Furthermore, from the detected changes of the atomic fractions of the C 1s and O 1s core level components it can be deduced that the stoichiometry of the introduced dopant species decreases from TiO_4 for the U(600)Ti$_1$ sample over $TiO_{2.5}$ for U(600)Ti$_3$ to TiO_2 for U(600)Ti$_5$ indicating a increasing interaction between the Ti groups.

The position of the symmetric N 1s peak (not shown here), characteristic for the urea structure, remains unchanged at 400.2 eV for all samples. The binding energy of the Ti 2p$_{3/2}$ peak (not shown either) increases only slightly with the Ti content from 459.1 to 459.4 eV, an energy range compatible with the 4+ oxidation state.

The derived structural model suggests that titanoxane species should be formed for the lowest doping concentration (U(600)Ti). Furthermore, a chemical equilibrium involving acac molecules coordinating to Si^{4+} seems to occur. Interestingly enough, the existence of such equilibrium between Ti-acac and Si-acac should hinder the condensation degree of the siloxane species, as suggested by SAXS results exposed below. For the samples with high Ti content (U(600)Ti$_5$), the increasing interaction between the Ti groups leads to a TiO$_2$ stoichiometry, indicating the presence of TiO$_x$ clusters, embedded in the cross-linked hybrid matrix. Due to the inclusion of the Ti^{4+} complex there is a decrease of the hybrid network connectivity. Furthermore it is proposed that the introduced excess carbon and oxygen (Table 1), including hydrocarbons, carboxyl groups and terminating C-OH groups, bond at surface of these nano-clusters. The formation of TiO$_x$ clusters in the hybrid matrix is also supported by results obtained from the analysis of the SAXS data, presented below.

Small Angle X-ray Scattering (SAXS)

Experimental SAXS profiles I(q) obtained for the pure U(600) hybrid and the U(600)Ti$_1$ and U(600)Ti$_5$ samples are shown in Figure 5. All curves contain a single peak with the position of the maximum depending on the titanium content. This peak has already been observed in di-ureasil hybrids and attributed to an interference effect

in the X-ray scattering amplitude produced by the spatial correlation between siloxane clusters or particles to which polymer chain ends are grafted.[11]
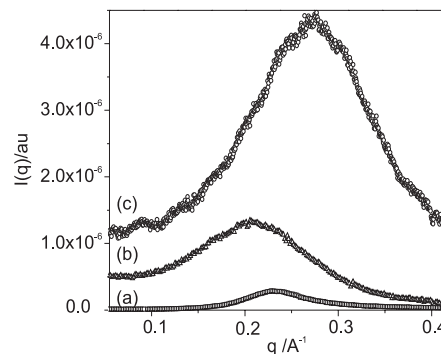

Figure 5. SAXS patterns for (a) U(600); (b) U(600)Ti$_1$ and (c) U(600)Ti$_5$.

In such a system constituted of clusters with a electronic density ρ_1 embedded in a homogeneous matrix with a density ρ_2, the degree of order of the clusters arrangement can be obtained from the width of the interference peak. An average size of the correlation volume, L_c, associated with spatial distribution of clusters (*i.e.*, an estimate of the size of very disordered "supercrystal") can be obtained by applying the Scherrer equation in the case of small-angle X-ray scattering:

$$L_c = 4\pi / \Delta q \qquad (1)$$

where Δq is the full width at half-maximum (FWHM) of the correlation peak of the SAXS curve.

The average distance between clusters, d_s, can be estimated by using the following equation:

$$d_s = 2\pi / q_{max} \qquad (2)$$

q_{max} being the modulus of the scattering vector corresponding to the maximum intensity.[12]

Additional information was inferred from SAXS data plotted in Figure 5. Assuming an isotropic hybrid structure with a constant electronic density ρ_1, of the inorganic phase embedded in a homogeneous polymer matrix (ρ_2) the integral Q of the scattering function (the "invariant") is given by:[12]

$$Q = \int_0^\infty I(q)q^2 \, dq = 2\pi^2 (\rho_1 - \rho_2)^2 \, \phi_1 \phi_2 \, V \qquad (3)$$

where ϕ_1 and ϕ_2 are the total volume fractions of inorganic clusters and polymer matrix, respectively, and V is the irradiated volume.

The asymptotic behavior at high q of the scattering function I(q) is given by:[12]

$$A_p = \lim I(q) \, q^4 = 2\pi (\rho_1 - \rho_2)^2 \, S \qquad (q \to \infty) \qquad (4)$$

where A_p is the Porod's constant, and S is the interface area between the two phases.

The ratio Q/A_p yields the average radius R_p of a spherical and monodisperse set of particles:

$$Q/A_p = \pi \phi_1 \phi_2 (V/S) = \pi \phi_2 (V'/S) = \pi \phi_2 R_p/3 \qquad (5)$$

where V' is the total volume of the minor phase (the inorganic particles). In systems with a small volume fraction ϕ_1 of particles, we have $\phi_2 \sim 1$ and so equation (5) can be approximated by

$$Q/A_p = p \, R_p/3 \qquad (6)$$

The XPS data suggest that at low titanium content (U(600)Ti$_1$) Ti^{4+} based species are essentially bonded to neighboring siloxane groups. Therefore, as a first approximation, we can consider the hybrid as constituted of two phases: (*i*) inorganic-rich phase located at PEO chains ends constituted by siloxane inorganic particles and neighboring Ti^{4+} species; (*ii*) polymeric organic matrix. Furthermore, for low titanium content the hybrid can be considered as a "diluted" system, since the volume fraction of the inorganic phase embedded in the polymer matrix (calculated from composition parameters) is around 20%. Consequently the formalism described by equations (1) to (6) can be applied. The analysis of the scattering profiles (Figure 5), led to the values of the invariant Q, Porod's constant A_p, the average inorganic particle radius R_p, the average interparticle distance d_s and the average size of the correlation volume L_c, as reported in Table 2. A decrease of the average radius of inorganic particles R_p from 6 Å to 3.5 Å is observed from the U(600) hybrid to the U(600)Ti$_1$ sample. This behavior is consistent with XPS measurements which suggest the formation of a chemical equilibrium between Ti-acac and Si-acac species, which should hinder the efficiency of the polycondensation reactions of silicon species, resulting on a smaller average inorganic particles radius. At this point it should be pointed out that if the dispersion in the size of the collection of scattering particles is high, Rp values could differ significantly from the real values.

In addition, Figure 5 and Table 2 show an increase of the invariant Q (scattered intensity) and of the Porod's constant A_p from the U(600) hybrid to the U(600)Ti$_1$ sample. Since the average inorganic particle radius decreases this behavior can be attributed to an increase in electronic density contrast ($\rho_1 - \rho_2$) between the inorganic particles and the polymer matrix (equations (3) and (4)). Again, this interpretation is consistent with the bonding of Ti^{4+} based species to siloxane groups suggested by XPS measurements.

Table 2. Invariant Q, Porod's constant A_p, average inorganic particle radius R_p, average interparticle distance d_s and average size of the correlation volume L_c obtained from SAXS measurements for the sample U(600), U(600)Ti$_1$ and U(600)Ti$_5$

sample	Q(arb.units)	A_p (arb.units)	R_p(Å)	d_s(Å)	L_c(Å)
U(600)	3.2×10^{-9}	4.6×10^{-10}	6	28	140
U(600)Ti$_1$	1.2×10^{-8}	3.4×10^{-9}	3.5	30	125
U(600)Ti$_5$	1.5×10^{-6}	3.7×10^{-7}	3.9	23	71

Figure 5 shows for the sample with the lowest Ti concentration a shift of the peak position toward lower q values associated with an increase of the inorganic interparticle distance d_s from 28 Å to 30 Å (Table 2). This behavior reveals that PEO chains acquire a more extended conformation by introducing a small quantity of titanium. In fact, vibrational analysis has suggested the disruption of the Urea-PEO interactions that could be related to this new conformation.

The nanostructural features of the hybrid containing high titanium content (U(600)Ti$_5$) differ considerably from the U(600)Ti$_1$ sample. As a matter of fact, a strong increase of the peak width reveals a pronounced diminution of the spatial correlation between inorganic particles in this more concentrated material. This behavior supports the XPS results suggesting the formation of titanium-based nanoclusters in the polymer matrix at high titanium concentration. These clusters may result from the hydrolysis and polycondensation of the 9 titanium alcoxide molecules per PEO chain present in the initial sol. In fact, in this system both titanium-based clusters and siloxane-based ones should contribute to X-ray scattering. Due to the presence of three phases in the Ti rich composite the two electronic density-model loses its validity and consequently the use of equations (1) to (4) to determine structural parameters is not allowed. However, taking into account that the atomic concentration of Ti is 5 times higher than that of Si and also that the electronic density contrast of titanium in respect to polymer matrix is quite higher than that of Si (density of TiO$_2$ is 4.23 g cm^{-3} and of silica 2.2 g cm^{-3}), a two electronic density-model consisting on titanium-based clusters embedded in the PEO matrix can be considered as a reasonable approximation. Considering that the average inorganic particles radius of about 4 Å (Table 2), calculated taking into account this two-density model, corresponds to a titanium oxide nanocluster, then an average number of only one titanium oxide-based nanocluster per PEO chain should be formed, which is similar as existing for siloxane particles in the undoped hybrid. Consequently the observed diminution of the inorganic intercluster distance from 30 to 23 Å (Table 2) reveals the existence of a more concentrated system of inorganic particles in the U(600)Ti$_5$

sample. The clear diminution of the spatial correlation between inorganic particles in this sample, illustrated by the pronounced decrease of Lc (Table 2), can be explained by the fact that titanium-based clusters are randomly embedded in the PEO matrix. This situation is clearly different from the siloxane-based particles responsible for X-ray scattering in the undoped and U(600)Ti$_1$ nano-composites where correlation is evident.

Finally, the pronounced increase of the scattered intensity of the U(600)Ti$_5$ observed in Figure 5 can be attributed to the increase of the electronic density contrast due to the larger density of titanium-based clusters existing in this sample in respect with the siloxane-based ones present in U(600)Ti$_1$.

Waveguides

Table 3 shows the results obtained for the optical parameters of the hybrid waveguides deposited on glass substrates. The refractive index of the borosilicate substrate for both TE and TM polarization was 1.5237, 1.5194 and 1.5043 at 543.5, 632.8 and 1550 nm, respectively. The planar waveguides support various propagation modes in the visible region and one propagation mode in the near infrared region. With increasing the Ti^{4+} concentration a decrease in thickness was observed, ranging from 3.3 μm for the sample U(600)Ti$_1$ to 1.5 μm (U(600)Ti$_5$). As expected, also an increase in refractive index was detected. Sorek *et al.* [13] studied organic-inorganic hybrids using GLYMO (γ-gycidyloxipropyltrimethoxysilane) and Ti(OPr^i)$_4$ and obtained similar behavior for thickness and refractive index. These authors observed a linear increase of the refractive index, *n*, at 632.8 nm as a function of the Ti^{4+} content (n(X)= 1.42 + 0.28X where X is the Ti molar fraction). Considering these results a *n* value of ~1.65 would be expected for the U(600)Ti$_5$ sample. The slightly

lower value, observed in Table 3, is probably related to the higher organic fraction in our samples. [13]

Figure 6 shows the refractive index profile reconstructed from the effective indices at 632.8 nm by an inverse Wentzel-Kramers-Brillouin method. [14]

The small difference of the refractive index profiles obtained for TE and TM modes indicates that the birefringence in this waveguide is negligible. Interesting enough, samples do not exhibit a single step profile with a uniform refractive index throughout the thickness as observed before for example in GLYMO-HfO$_2$ systems. [15] Since composition inhomogeneities are not expected, the observed gradient of the refractive index is most probably related to the inhomogeneous density throughout the sample. These density inhomogeneities could be the result of the drying process, which is more efficient in the surface region of the sample. These effects will be the subject of future publications since the prism coupling technique could then be applied in order to check homogeneity in thin films.

Figure 7 shows the squared electric field profiles of the TE$_0$ mode calculated for 632.8 and 1550 nm using the parameters obtained by the m-line measurements for 3 samples. The confinement of the injected light can be obtained by the ratio of integrated intensity, *i.e.* the square of the electric field, at 632.8 nm in the waveguide and the total intensity, which includes also the squared evanescent fields. Values between 0.98 and 0.99 were obtained. For the 1550 nm wavelength the confinement coefficients are between 0.8 and 0.96. The results show that an efficient injection is possible at these wavelengths.

Table 3. Optical parameters measured at 543.5, 632.8 and 1550 nm for TE polarization for Ti^{4+} containing siloxane-PEO planar waveguides on soda-lime substrates labeled as U(600)Ti$_1$, U(600)Ti$_3$ and U(600)Ti$_5$

| Sample	U(600)Ti$_1$	U(600)Ti$_3$	U(600)Ti$_5$
molar ratio [Ti]:[Si]	1:1	3:1	5:1
n at 543.5 nm (± 0.0005)	1.5412	1.6065	1.6352
n at 632.8 nm (± 0.0005)	1.5346	1.5960	1.6220
n at 1550 nm (± 0.0005)	1.5212	1.5616	1.5909
thickness (± 0.1 μm)	3.3	2.0	1.5
attenuation coefficient at 632.8 nm (± 0.1dB cm^{-1})	1.5	1.7	2.1
attenuation coefficient at 1550 nm (± 0.1dB cm^{-1})	0.2	0.4	0.4
number of modes at 543.5 nm	4	4	3
number of modes at 632.8 nm	3	3	3
number of modes at 1550 nm	1	1	1
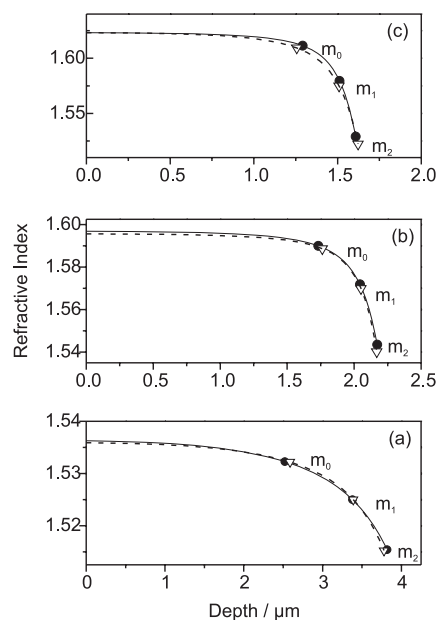
Figure 6. Refractive index profiles of the U(600)Ti$_1$ (a), U(600)Ti$_3$ (b), and U(600)Ti$_5$ (c) planar waveguides reconstructed from modal measurements at 632.8 for TE (straight line) and TM (dash line) polarization. The effective indices of the TE (•) and TM (∇) modes are reported.
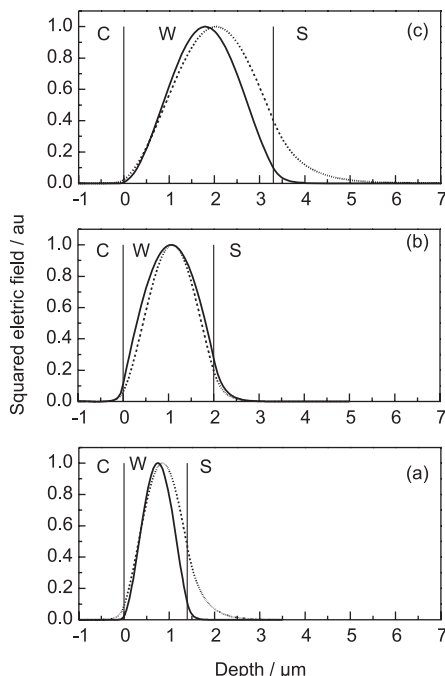
Figure 7. Calculated square electric field profiles of the TE_0 mode at 1550 nm (dash line) and 632.8 nm (straight line) of the waveguides across the layered structure-cladding of air C, waveguide W, and the soda-lime substrate S of the planar waveguide.

Conclusions

Novel organic-inorganic hybrid planar waveguides in the visible and infrared range were obtained from Ti^{4+}-acac-ureasil sols deposited on glass substrates. Structural investigation by Raman, FT-IR, XPS and SAXS measurements show that starting from the pure di-ureasil hybrid the addition of β-diketonate stabilized Ti^{4+} sol (Ti/Si molar ratio ≈ 1) induces an interaction between the titanium species and the siloxane phase, inhibiting polycondensation of silicon species and leading to the breaking of urea-oxyethylene interactions. Further addition of Ti^{4+} sol (up to Ti:Si molar ratio 5:1) leads to the formation of TiO_2 nanoclusters embedded in the hybrid matrix. The optical characterization of the waveguides reveals an increase of the refractive index with increasing titanium content. The planar waveguides present thickness of a few microns adequate for technological applications and support well confined propagating modes with low attenuation loss.

Acknowledgments

Supplementary Information

Typical output of the prism couples apparatus is available free of charge as PDF file at http://jbcs.sbq.org.br

References

1. Sanchez, C.; Ribot, F.; *Proceedings of the First European Workshop on Hybrid Organic-Inorganic Materials*, special issue of *New J. Chem.* **1994**, *18*.

2. Novak, B.; *Adv. Mater.* **1993**, *5*, 422.

3. Schmidt, H.; Kaiser, A.; Patzelt, H.; Sholze, H.; *J. Phys. Colloq.* **1982**, *C9*, 275.

4. de Zea Bermudez, V.; Carlos, L. D.; Alcácer, L.; *Chem. Mater.* **1999**, *11*, 569.

5. Dahmouche, K.; Atik, M.; Mello, N. C.; Bonagamba, T. J.; Paneppucci, H.; Aegerter, M. A.; Judeinstein, P.; *J. Sol-Gel Sci. Technol.* **1997**, *8*, 711.

6. Carlos, L. D.; Messaddeq, Y.; Brito, H. F.; Ferreira, R. A. S.; Bermudez, V. D.; Ribeiro, S. J. L.; *Adv. Mater.* **2000**, *12*, 594.

7. Bermudez, V. D.; Ferreira, R. A. S; Carlos, L. D.; Molina, C.; Dahmouche, K.; Ribeiro, S. J. L.; *J. Phys. Chem. B* **2001**, *105*, 3378.

8. Briggs, D.; Seah, M. P. In *Practical Surface Analysis, vol. 1, Auger and X-ray photoelectron spectroscopy*; J. Wiley & Sons: Chichester, 1996.

9. Moulder, J. F.; Stickle, W. F.; Sobol, P. E.; Bomben, K. D. J.; Chastain, eds.; *Handbook of X-ray Photoelectron Spectroscopy: A Reference Book of Standard Spectra for Identification and Interpretation of XPS Data*; Perkin-Elmer, Physical Electronics Division, 1992.

10. Lassaletta, G.; Fernández, A.; Espínos, J. G.; González-Elipe, A. R.; *J. Phys. Chem.* **1995**, *99*, 1484.

11. Dahmouche, K.; Santilli, C. V.; Pulcinelli, S. H.; Craievich, A. F.; *J. Phys. Chem. B* **1999**, *103*, 4937.

12. Glatter, O.; Kratky, O.; *Small-Angle X-ray Scattering*, Academic Press: New York, 1982.

13. Sorek, Y.; Reisfeld, R.; Finkelstein, I.; Ruschin, S.; *Appl. Phys. Lett.* **1993**, *24*, 3256.

14. Chiang, K. S.; *J. Lightwave Technol.* **1985**, *LT-3*, 385.

15. Ribeiro, S. J. L.; Messaddeq, Y.; Gonçalves, R. R.; Ferrari, M.; Montagna, M.; Aegerter, M. A.; *Appl. Phys. Lett.* **2000**, *22*, 3502.

Supplementary Information

Structure and Properties of Ti⁴⁺-Ureasil Organic-Inorganic Hybrids

Celso Molina,[a] Karim Dahmouche,[a] Peter Hammer,[a] Verónica de Zea Bermudez,[b] Luís D. Carlos,[c] Maurizio Ferrari,[d] Maurizio Montagna,[e] Rogéria R. Gonçalves,[f] Luiz. F. C. de Oliveira,[g] Howell. G. M. Edwards,[h] Younes Messaddeq[a] and Sidney J. L. Ribeiro[,a]*

[a]*Instituto de Química, Universidade Estadual Paulista, CP 355, 14801- 970 Araraquara – SP, Brazil*

[b]*Departamento de Química, Universidade de Trás-os-Montes e Alto Douro, Quinta dos Prados, 5001 Vila Real Codex, Portugal*

[c]*Departamento de Física, Universidade de Aveiro, 3810 Aveiro, Portugal*

[d]*CNR-INF, Instituto di Fotonica i Nanotecnologie, CSMFO Group, via Sommarive 14, 38050, Povo (TN), Italy*

[e]*IDipartimento di Fisica, Università di Trento, CSMFO Group, via Sommarive 14, 38050 Povo, (TN), Italy*

[f]*Departamento de Química, Universidade de São Paulo, 14040-901 Ribeirão Preto – SP, Brazil*

[g]*Departamento de Quimica, Universidade Federal de Juiz de Fora, 36036-900 Juiz de Fora – MG, Brazil*

[h]*Department of Chemical and Forensic Sciences, University of Bradford, Bradford, BD7 1 DP, UK*
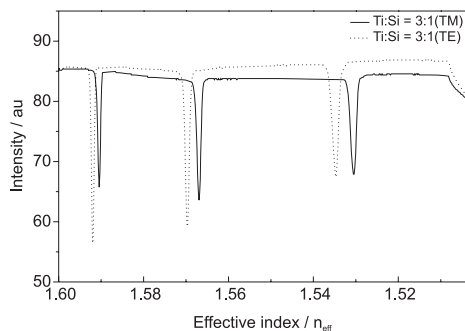
Figure 1S. Typical output of the prism couples apparatus.

The above figure is a typical output of the prism coupler apparatus. It gives the guided modes for one of the organic-inorganic thin films studied in this paper as a function of the effective index.

The effective index n_{eff} is given by

$$n_{eff} = \frac{\beta_m}{\vec{k}} \qquad (1)$$

where k is the wavevector of the incident light and β_m is the propagation constant, of the mode m, given by

$$\beta_m = nksin\theta \qquad (2)$$

i.e., it is the projection of the radiation wavevector along the propagation direction.

From a set of effective indexes a continuous effective-index function is defined by Chiang.[1] That function is then used to construct a refractive index profile by numerically solving the equation proposed in the inverse Wentzel-Kramers-Brillouin method.[1] This approach is used by the Metricon apparatus with the algorithm defined by Chiang.[1] Figure 6 of the paper is obtained in this way.

Figure 7 of the paper shows the calculated electric field confinement in the waveguide and also the evanescent field in the clading (substrate and air). It is calculated with a home-made software written by the authors, with data obtained from m-lines measurement. Basic formulae can be found in standard bibliography for waveguides.[2] The software is available from the authors under request.

1. Chian, K.S.; *J. Lightwave Technol.* **1985**, *LT-3*, 385.

2. Marcuse, D.; *Theory of Dielectric Optical Waveguides*, 2ⁿᵈ ed., Academic Press, 1991.

* e-mail: sidney@iq.unesp.br